LA-UR-17-30221
Approved for public release; distribution is unlimited.

Title: Comparison of Experimental Methods for Estimating Matrix Diffusion Coefficients for Contaminant Transport Modeling

Author(s): Telfeyan, Katherine Christina
Ware, Stuart Douglas
Reimus, Paul William
Birdsell, Kay Hanson

Intended for: Report

Issued: 2017-11-06

Comparison of Experimental Methods for Estimating Matrix Diffusion Coefficients for Contaminant Transport Modeling

Katherine Telfeyan*

S. Doug Ware

Paul W. Reimus

Kay H. Birdsell

Earth and Environmental Sciences Division, Los Alamos National Laboratory, Los Alamos, NM 87545, United States
**Corresponding author Tel.: +1 505 665 3880*
E-mail address: ktelfeyan@lanl.gov

Abstract

Diffusion cell and diffusion wafer experiments were conducted to compare methods for estimating matrix diffusion coefficients in rock core samples from Pahute Mesa at the Nevada Nuclear Security Site (NNSS). A diffusion wafer method, in which a solute diffuses out of a rock matrix that is pre-saturated with water containing the solute, is presented as a simpler alternative to the traditional through-diffusion (diffusion cell) method. Both methods yielded estimates of matrix diffusion coefficients that were within the range of values previously reported for NNSS volcanic rocks. The difference between the estimates of the two methods ranged from 14 to 30%, and there was no systematic high or low bias of one method relative to the other. From a transport modeling perspective, these differences are relatively minor when one considers that other variables (e.g., fracture apertures, fracture spacings) influence matrix diffusion to a greater degree and tend to have greater uncertainty than diffusion coefficients. For the same relative random errors in concentration measurements, the diffusion cell method yields diffusion coefficient estimates that have less uncertainty than the wafer method. However, the wafer method is easier and less costly to implement and yields estimates more quickly, thus allowing a greater number of samples to be analyzed for the same cost and time. Given the relatively good agreement between the methods, and the lack of any apparent bias between the methods, the diffusion wafer method appears to offer advantages over the diffusion cell method if better statistical representation of a given set of rock samples is desired.

I. Introduction

Transport of radionuclides and other contaminants in saturated fractured rock can be strongly affected by diffusive mass transfer between fractures and the surrounding rock matrix, a process known as matrix diffusion (Grisak and Pickens, 1980; Neretnieks, 1980; Tang et al., 1981; Maloszewski and Zuber, 1985; Skagius and Neretnieks, 1986; Liu et al., 2004). Matrix diffusion is typically associated with "dual-porosity" systems in which flow is predominantly in fractures, but there is a significant amount of non-flowing (or very slowly-flowing) porosity in the surrounding rock matrix that is in diffusive communication with the flowing fractures (Reimus and Haga, 1999; Reimus et al., 2002a). This diffusive communication can result in significant retardation of both reactive and nonreactive solutes relative to groundwater travel times in the fractures. For non-reactive solutes, the effective retardation factor can theoretically approach the ratio of total porosity to flowing porosity, where the total porosity is the sum of the flowing porosity and the non-flowing porosity that is in diffusive communication with the flowing porosity (Reimus et al., 2011, Bradbury and Green, 1985). Reactive (sorbing) solutes will also experience this retardation, but their retardation will be magnified by the increased sorptive surface area that they come into contact within the matrix relative to what they would have contacted if they were confined to the flowing fractures (Grisak and Pickens, 1980; Robinson et al., 2012). Even low porosity granites can have significant matrix storage capacities, and thus diffusion can be an important mechanism affecting contaminant transport and retardation in such systems (Neretnieks, 1980; Reimus et al., 2003).

A large inventory of radionuclides is present underground at the Nevada Nuclear Security Site (NNSS) as a result of underground nuclear testing from the 1950s until 1992, and much of this inventory resides in saturated, fractured volcanic tuff and lava flow aquifers that have high fracture permeabilities (Blankennagel and Weir, 1973; Finnegan et al., 2016). Because of their high permeabilities, these aquifers may have relatively fast groundwater travel times from radionuclide source locations (i.e., nuclear test cavities). However, the majority of the saturated porosity in these aquifers is in the relatively impermeable rock matrix (Drellack et al., 1997; Reimus et al., 2002a, b), so the aquifers represent classic dual porosity systems in which matrix diffusion is potentially an important radionuclide retardation mechanism. Tritiated water (^{3}HHO) tends to dominate predicted offsite anthropogenic radioactivity in groundwater near the NNSS because of its large inventory and the fact that most other radionuclides present in the aftermath

of nuclear testing are either very low in solubility, strongly retarded and attenuated by geochemical processes, or present in such small amounts that they do not contribute much to potential radiological doses even if little credit is taken for retardation processes. ^{3}HHO has been detected in wells outside the boundaries of the NNSS (Farnham and Rehfeldt, 2017; Navarro, 2017). Because matrix diffusion has a big potential impact on ^{3}HHO transport, considerable work has been conducted to estimate matrix diffusion coefficients of non-reactive solutes in NNSS rocks (Reimus and Haga, 1999; Reimus et al., 2002a, b; Reimus et al., 2007).

Although the ratio of total porosity to fracture porosity defines the upper limit of the retardation factor of a non-reactive solute in a dual-porosity system, the matrix diffusion coefficient is needed to estimate diffusive mass transfer rates, which affect both breakthrough times and peak concentrations (Reimus et al., 2002b), and thus contaminant boundary calculations, which delineate the possible extent of radionuclide-contaminated groundwater from underground nuclear testing. The matrix diffusion coefficient is the product of the solute's free water diffusion coefficient and the matrix tortuosity. Unambiguous estimates of matrix diffusion coefficients are best determined in laboratory tests (Callahan et al., 2000; Reimus et al., 2007). Although field tracer tests can be used to obtain valuable information on matrix diffusion, they can only yield estimates of a lumped mass transfer coefficient for matrix diffusion, which also depends on porosity and fracture aperture, not a direct matrix diffusion coefficient estimate (Reimus et al., 2003).

Laboratory estimates of matrix diffusion coefficients are traditionally determined using a through-diffusion method, whereby a reservoir containing the tracer of interest is separated from a receiving reservoir by a rock sample of known thickness and cross-sectional area, and the concentration change of the receiving reservoir is monitored through time (e.g., Bradbury and Green, 1985; Skagius and Neretnieks, 1986; Reimus et al., 2007). However, this through-diffusion method can be expensive, time consuming, and complex, limiting the number of samples that can be analyzed. Another method, involving the diffusion of a tracer "out of" a rock sample saturated with tracer solution into an initially tracer-free reservoir in which the sample is immersed may provide a cheaper, quicker, and simpler alternative because this method does not require the use of a specialized diffusion cell, and it permits diffusion from both sides of the rock wafer, thus expediting the tracer breakthrough times (Reimus et al., 2006; Hershey and Fereday, 2016). This study compares the merits of these two methods.

II. Methods

II.A. Sample Descriptions

Rock core samples were obtained from corehole UE-20c, located on Pahute Mesa at the NNSS, where previous studies have been conducted to evaluate radionuclide migration from underground nuclear tests (Reimus et al., 2002a, b, 2003, 2007; Liu et al., 2004; Robinson et al., 2012). The selected core samples were subsampled to avoid fractures or major voids and cut into pieces of intact matrix material of constant thickness and cross-sectional area (Figure 1), which are hereafter referred to as wafers. These samples represent different hydrostratigraphic units that have significant transmissivity within Pahute Mesa, and for which matrix diffusion coefficient data were lacking before this study. The Benham Aquifer cores represent variable sizes of lithophysal cavities within a similar matrix in this lava flow unit from depths of 1189, 1353, and 1925 feet below ground surface (bgs). Previous work demonstrated that the lithophysal cavities are open to exchange with fracture networks and act to retard the flow of water through vertical fractures (Liu et al., 2004). The lithophysal cavities in the Benham Aquifer samples are largely filled with poorly consolidated alteration minerals, so they are not void spaces, although they appear to be more porous and hence more accessible to diffusion than the surrounding lava matrix. Duplicate Tiva Canyon Aquifer (TCA) samples represent the moderate-to-densely welded tuff at 2131 feet bgs (Table 1). Use of these duplicate samples located adjacent to each other in this core sample provides a measure of experimental reproducibility.

Sample ID/ Depth	HGU	Rock Type	Area (cm^2)	Thickness (cm)	φ	Pore Volume (cm^3)	K ($cm\ sec^{-1}$)	k (m^2)
UE-20c-2131.3-2131.5 A	TCA	Welded Tuff	94.52	1.95	0.181	34.3	$1.47 \cdot 10^{-8}$	$1.50 \cdot 10^{-17}$
UE-20c-2131.3-2131.5 B	TCA	Welded Tuff	87.85	3.06	0.179	49.5	$2.45 \cdot 10^{-8}$	$2.50 \cdot 10^{-17}$
UE-20c-1925.1-1925.3	BA	Lava Flow; lithophysae poor	43.92	5.54	0.143	35.3	$5.00 \cdot 10^{-7}$	$5.11 \cdot 10^{-16}$
UE-20c-1353-1353.28	BA	Lava Flow; lithophysae rich	86.78	6.19	0.161	92.4	$2.68 \cdot 10^{-6}$	$2.74 \cdot 10^{-15}$
UE-20c-1189-1189.25	BA	Lava Flow lithophysae moderate	93.94	6.22	0.133	83.5	$3.87 \cdot 10^{-5}$	$3.95 \cdot 10^{-14}$

Table 1: Measured properties of UE-20c rock samples used in diffusion studies. The relative amounts of lithophysae (i.e., rich, moderate, poor) in the lava flow samples were determined visually.

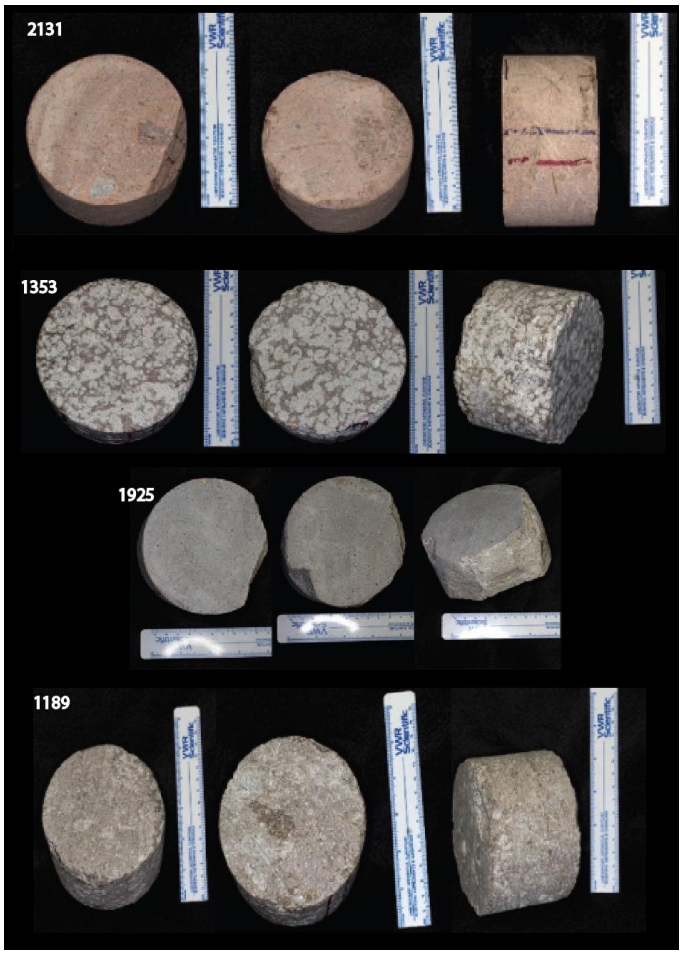

Figure 1: Photographs of UE-20c rock wafers from Pahute Mesa used in diffusion cell and diffusion wafer experiments. Additional photos are shown in the appendix.

II.B. Porosity and Permeability

Prior to diffusion testing, the porosity of the rock wafers was measured by dividing the difference between their saturated and oven-dry weights by the known sample volume, assuming a water density of 1 g/cm^3. Each sample was then incorporated into a diffusion cell apparatus (see II.C.i), and its permeability was measured using either the constant head method (for the higher-permeability Benham Aquifer lava flow samples) or the falling head method (for the lower permeability Tiva Canyon tuff samples; Freeze and Cherry, 1979). The constant and falling head methods provided hydraulic conductivity estimates, from which permeability was determined according to,

$$k = \frac{K \cdot \mu}{\rho \cdot g} \qquad \text{(eq 1)}$$

in which K is hydraulic conductivity, μ is the dynamic viscosity of water, ρ is density of water, and g is acceleration due to gravity (Callahan et al., 2000).

II.C. Experiment 1. Diffusion Cell: Diffusion through rock wafer

II.C.i. Assembly of Diffusion Cell Apparatus

Details of the experimental methods are provided in Callahan et al. (2000), Reimus et al. (2002a, b), and Reimus et al. (2007). Briefly, each rock wafer was placed in a square mold into which Room Temperature Vulcanization (RTV) silicone was poured until it covered the edges of the wafers without spilling over onto the top surface. After setting, the silicone serves as a gasket material that can be easily sealed between two reservoirs. A primer was used to achieve a good seal between the silicone and the periphery of each rock wafer to ensure that diffusion was only through the rock matrix and not along the edges of the wafers. Care was taken to ensure no silicone came in contact with either of the open faces of the rock.

Los Alamos municipal tap water was used in all experiments and was filter sterilized (0.2 μm). Rock wafers were saturated with filtered tap water under vacuum after flushing the vacuum chamber with CO_2 multiple times. Replacing atmospheric gas with CO_2 expedites water saturation, as CO_2 dissolves much more readily in water than does air (Callahan et al., 2000; Reimus et al., 2006). Once there were no visible bubbles escaping the samples, the samples were assumed to be saturated (~ 1 week). Wafers were then immediately placed in between two reservoirs machined out of plexiglass, which were rapidly secured with screws and filled with water to maintain saturation. The apparatus was oriented horizontally, and the water level on both sides of the reservoir was kept identical to eliminate the potential for advective flow (Figure 2). Both reservoirs were kept well mixed using a magnetic stir bar (Reimus et al., 2002a, b).

II.C.ii. Tracer Introduction, Sampling, and Measurements

Tritium was chosen as the nonsorbing solute with which to measure matrix diffusion coefficients. The free-water diffusion coefficient (D*) of ^3HHO is $2.4 \cdot 10^{-9}$ m^2 s^{-1} (Kozaki et al., 1999; Reimus et al., 2007). Between 0.3-0.6 mL of a stock solution of ^3HHO (2,550,581 cpm mL^{-1}) was added to the large chamber of each cell to obtain an initial concentration (C_i) of ~ 1,300 cpm mL^{-1}. Samples from both the large (tracer reservoir; 800-1600 mL capacity) and small (collection reservoir; 90-200 mL capacity) chambers were obtained daily thereafter.

Approximately 0.5 mL of water was sampled by syringe from the small chamber, whereas 5 mL of sample was extracted by syringe from the large chamber to maintain constant head levels on each side. Concentration changes in the large chambers were small relative to the starting concentrations, so only the data from the small chambers were used to determine diffusion coefficients.

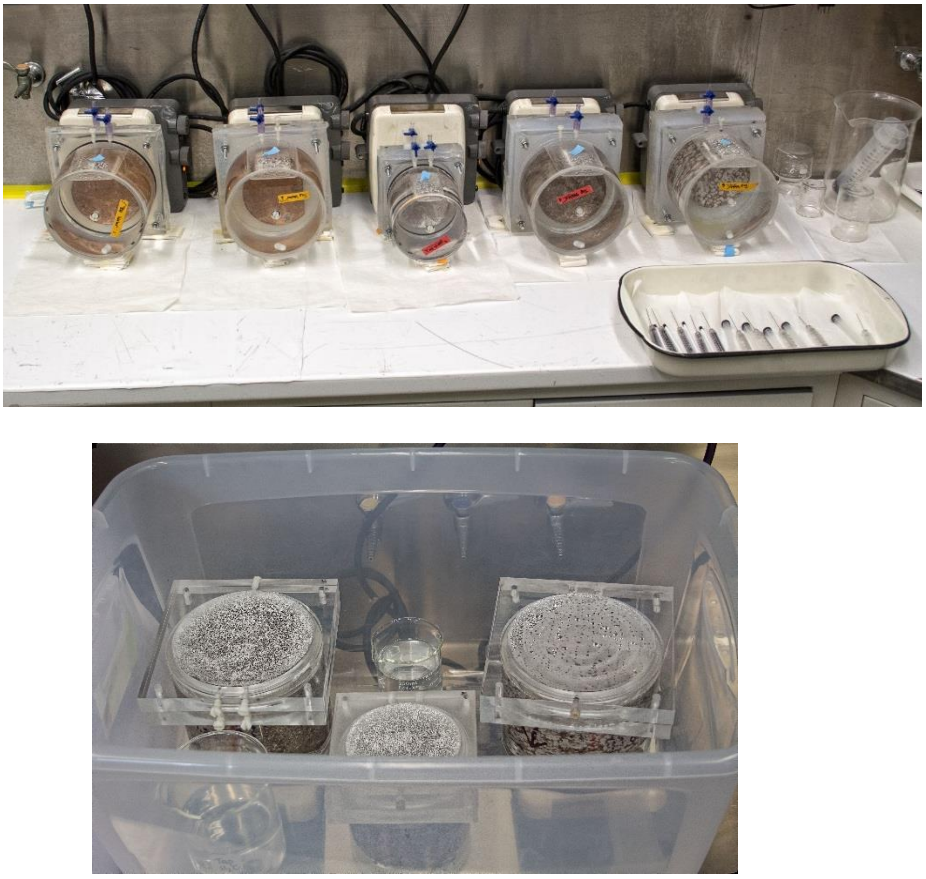

Figure 2: Set-up of diffusion cell (top) and diffusion wafer (bottom) experiments.

^{3}HHO activity was measured using a Packard Tri-Carb 2500 liquid scintillation counter. The 0.5 mL samples were diluted to 6 mL with deionized water, and then 14 mL of Ultima Gold scintillation cocktail was added (Reimus et al., 2002b). Standards prepared with different ratios of water to cocktail were used to obtain a quench curve to correct for variations in scintillation counting efficiencies of the samples caused by minor variations in water to cocktail ratios (Thomson, 2001).

II.C.iii. Calculation of Matrix Diffusion Coefficients from Diffusion Cell Method

Encapsulating the sides of the wafers with silicone ensured that bulk diffusion occurred in the axial direction, not radially (Reimus et al., 2006; Hershey and Fereday, 2016). Therefore, the matrix diffusion coefficients are determined by the 1-D diffusive transport equation:

$$\frac{\partial C}{\partial t} = \frac{D_m}{R_m} \cdot \frac{\partial^2 C}{\partial x^2} \qquad \text{(eq 2)}$$

in which C is the tracer concentration (cpm,), D_m is the diffusion coefficient (cm^2 sec^{-1}), R_m is the retardation factor (1 for nonsorbing solutes such as ^3HHO), x is the distance (cm), and t is time (sec) (Skagius and Neretnieks, 1986; Callahan et al., 2000; Reimus et al., 2002b). The tracer concentrations at the inlet and outlet boundary vary with time according to

$$\frac{\partial C_i}{\partial t} = \frac{\varphi \cdot A_w \cdot D_m}{V_i} \cdot \frac{\partial C}{\partial x}\Big|_{x=0} \qquad \text{(eq 3)}$$

$$\frac{\partial C_o}{\partial t} = -\frac{\varphi \cdot A_w \cdot D_m}{V_o} \cdot \frac{\partial C}{\partial x}\Big|_{x=L} \qquad \text{(eq 4)}$$

in which A_w is the cross-sectional area of the wafer, C_i is the tracer concentration in the large reservoir (inlet), C_o is the tracer concentration in the small reservoir (outlet), V_i and V_o are the volumes (mL) in the inlet and outlet reservoirs, respectively, φ is matrix porosity, and L is the rock wafer thickness (cm). In equations 3 and 4, the minor decreases in volumes of the inlet and outlet reservoir associated with sampling are ignored. Equations 2-4 were solved numerically using the DiffCell computer code, which employs an implicit finite-difference method (Reimus et al., 2002b). The matrix diffusion coefficient (D_m) is manually varied until the sum of squares of the differences between the modeled $C_o(t)/C_i(0)$ and the experimental $C_o(t)/C_i(0)$ is minimized (where $C_i(0)$ is the initial concentration in the large reservoir).

<u>II.D. Experiment 2.</u> Diffusion Wafers: Diffusion out of rock wafer

II.D.i. Assembly of Diffusion Wafers

The same rock wafers from the diffusion cell experiments were used in the subsequent diffusion wafer experiments. Upon completion of the tritium breakthrough experiments (through-diffusion), the diffusion cells were taken apart and the rocks dried for several days in an oven (105°C) to ensure complete dryness. The sides of the rocks were then resealed with silicone

to prevent contact between the sides of the rock and the water. The water used to saturate the wafers was spiked with deuterium (6,600‰) rather than tritium to avoid a radiological hazard during the vacuum saturation process (see II.C.i), which is prone to splashing and spillage.

The large chambers from the diffusion cell apparatus were used as cylindrical containers for the diffusion wafer experiments, and the small chambers were placed on top as a lid to minimize evaporation. Each wafer was placed in a separate container and completely immersed in filtered tap water. The wafers were suspended above the bottom of the containers by placing them on inverted perforated septum caps that were made of very thin aluminum so that there was negligible contact area between the septum caps and the wafers. In addition to providing unhindered diffusion access to the bottom surface of the wafers, the caps created space for magnetic stir bars below the wafers (Figure 2; Reimus et al., 2006; Hershey and Fereday, 2016). The containers were placed alongside open beakers of water inside larger plastic storage bins that were kept closed (except during sampling) as a further measure to minimize evaporation (Figure 2).

II.D.ii. Tracer Sampling and Measurement

Samples of the tap water surrounding the wafers were taken daily for the first 2 weeks and periodically thereafter. Approximately 2 mL of the tap water was collected for each sample. Deuterium samples were analyzed using isotope ratio mass spectrometry (IRMS) on a GV Instruments Eurovector Elemental Analyzer. Results are reported in δ notation as the per mil deviation (‰) relative to Vienna Standard Mean Ocean Water (VSMOW). δD values were calibrated using in-house standards calibrated to IAEA (International Atomic Energy Agency) standards VSMOW, SLAP (Standard Light Antarctic Precipitation), and GISP (Greenland Ice Sheet Precipitation), and although enriched samples fell outside the range of commercially available standards, a check standard (prepared at 10,000‰) yielded results within 1% of its calculated value.

II.D.iii. Calculation of Matrix Diffusion Coefficients from Wafer Diffusion Method

Matrix diffusion coefficients were again calculated using equation 2 with the following boundary conditions:

$$\frac{dC_i}{dx} = 0 \text{ at } x=0 \text{ (wafer midpoint)} \qquad \text{(eq 5)}$$

$$V_{res}\frac{dC_{res}}{dt} = -\varphi(2\cdot A_w)\cdot D_m\cdot\frac{\partial C}{\partial x}\ \text{at}\ x = 0.5\cdot T_w \qquad \text{(eq 6)}$$

in which C_i is the concentration of the tracer in the wafer (dD ‰ converted to ppm), x is the axial distance inside the wafer (cm), V_{res} is the volume of water in the container (mL), C_{res} is the tracer concentration in the container, t is time (s), φ is wafer porosity, A_w is the surface area of one side of the wafer (cm^2), D_m is the deuterium diffusion coefficient ($cm^2\ s^{-1}$), and T_w is the thickness of the wafer (cm). An explicit-in-time, finite-difference technique, coded in FORTRAN (Reimus et al., 2006; Hershey and Fereday, 2016), was used to obtain a solution that was fitted to the data. The matrix diffusion coefficient (D_m) was varied until the modeled breakthrough curve matched the experimental breakthrough curve (Hershey and Fereday, 2016).

III. Results

III.A. Porosities and Permeabilities

The measured matrix porosities and permeabilities of the 5 core samples are listed in Table 1. Although the porosity of the TCA welded tuff is slightly greater than that of the lava samples, the permeability of the tuff is 1 to 3 orders of magnitude less than that of the BA lava flow rocks containing lithophysal cavities. These measurements suggest that the lithophysal cavities tend to provide conduits for flow in the lava samples. The permeability, however, does not increase linearly as a function of lithophysal enrichment (Table 1). During the saturation process, it became apparent that there was a dominant discrete flow pathway in sample 1189 that probably corresponded to a partially-filled cavity that extended over most of the sample thickness. Consequently, the larger K value of sample UE-20c-1189-1189.25 relative to sample UE-20c-1353-1353.28, which had a higher density of lithophysal cavities, may reflect this single dominant feature. It was also noted that the cavities in sample UE-20c-1189-1189.25, though less numerous, tended to have more void space than those of sample UE-20c-1353-1353.28, which probably also influenced the permeabilities of the samples relative to each other.

III.B. Matrix diffusion coefficients

The matrix diffusion coefficients determined by fitting the data generated with the 2 experimental methods are shown in Table 2, and plots comparing the model matches to the data sets are shown in Figure 3. In this figure, concentrations are expressed as the concentration in the sampled reservoir divided by the initial concentration in either the source reservoir (diffusion cells) or the rock wafer (diffusion wafer). It is apparent in Figure 3 that the data sets are matched quite well by the respective models, and the goodness of fit of the models are acceptable. The diffusion wafer experiments were clearly conducted longer than necessary in most cases, as the diffusion coefficient estimates are determined primarily with data collected during the time period of increasing concentrations, not after the breakthrough curves reach their final plateaus (which are equal to the ratio of pore volume in the rock to the sum of the rock pore volume and the reservoir volume). Complete breakthrough occurred in the diffusion wafers in less than 1,000 hours, whereas the breakthrough curve had not plateaued after 1,500 hours in the diffusion cell experiments. Note that the diffusion wafer plots of Figure 3 are shown with a log time scale to emphasize the early breakthrough times of the experiments, which dictate the diffusion coefficient estimates. Deviations from concentration plateaus at later times in some of the diffusion wafer experiments were caused by cumulative errors in making corrections for extracted sample volumes. In the case of the diffusion wafer experiment for the sample from 1925 ft (UE-20c-1925.1-1925.3), the discontinuities at later times were caused by two additions of tap water to the reservoir, necessitated by a leak.

Sample ID/ Depth	**D_m ($cm^2\ sec^{-1}$) predicted from eq. 7**	**Fitted D_m ($cm^2\ sec^{-1}$) Diffusion Cell**	**Fitted D_m ($cm^2\ sec^{-1}$) Diffusion Wafer**	**% error $\frac{(Wafer-Cell)}{Cell}$**
UE-20c-2131.3-2131.5 A*	$8.25 \cdot 10^{-7}$	$2.40 \cdot 10^{-6}$	$2.05 \cdot 10^{-6}$	-15
UE-20c-2131.3-2131.5 B*	$9.02 \cdot 10^{-7}$	$2.50 \cdot 10^{-6}$	$2.15 \cdot 10^{-6}$	-14
UE-20c-1925.1-1925.3†	$1.37 \cdot 10^{-6}$	$2.63 \cdot 10^{-6}$	$2.05 \cdot 10^{-6}$	-22
UE-20c-1353-1353.28†	$2.03 \cdot 10^{-6}$	$2.30 \cdot 10^{-6}$	$2.95 \cdot 10^{-6}$	+28
UE-20c-1189-1189.25†	$2.98 \cdot 10^{-6}$	$2.07 \cdot 10^{-6}$	$2.70 \cdot 10^{-6}$	+30

* indicates welded tuff samples

† indicates lava flow samples

Table 2: Comparison of matrix diffusion coefficients predicted by equation 7 and determined by the diffusion cell and wafer methods.

As Table 2 shows, the differences between the estimated matrix diffusion coefficients from the two methods were always within ~30% of the diffusion cell estimate. There appeared to

be no systematic high or low bias of one method relative to the other. The diffusion cell method yielded greater diffusion coefficients for the duplicate tuff samples and one of the lava samples, whereas the diffusion wafer method yielded larger diffusion coefficients for two of the lava samples (Table 2). However, the results suggest that when matrix permeabilities are high, there may be a tendency to obtain smaller estimates from the diffusion cell experiments. More specifically, the two rocks with the highest permeability (i.e., UE-20c-1189-1189.25, UE-20c-1353-1353.28) yielded smaller estimates of D_m from the diffusion cell method as compared to the diffusion wafer method, and the sample with the highest permeability (i.e., UE-20c-1189-1189.25) yielded the smallest estimate of D_m applying the diffusion cell method. Of course, the limited sample size of this study does not permit definitive conclusions on such trends. The duplicate samples (UE-20c-2131.3-2131.5A and B) of different thickness show excellent agreement (within 5%) for a given method (Table 2), although the error between the two methods for the same samples was about 15%.

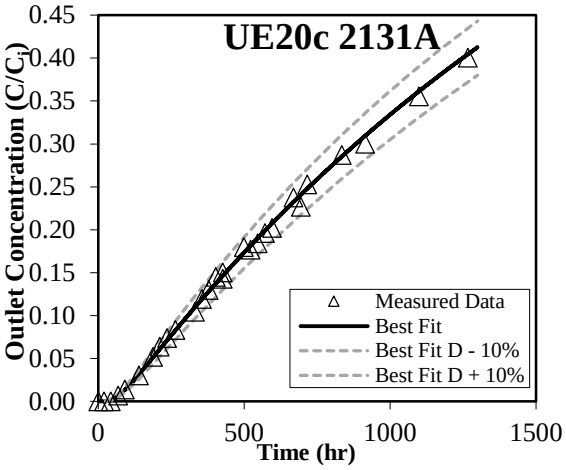
UE20c 2131A
Outlet Concentration (C/Ci)
Time (hr)
Measured Data
Best Fit
Best Fit D - 10%
Best Fit D + 10%

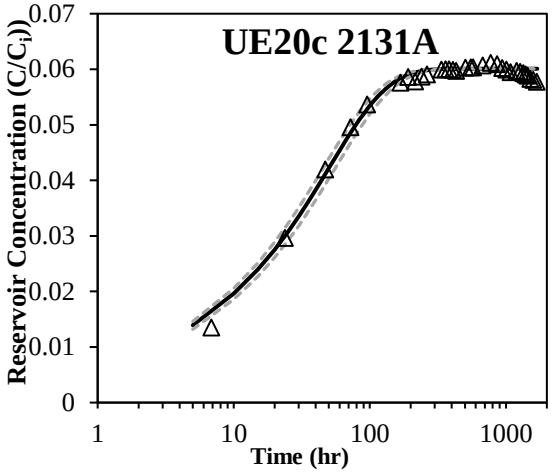
UE20c 2131A
Reservoir Concentration (C/Ci))
Time (hr)

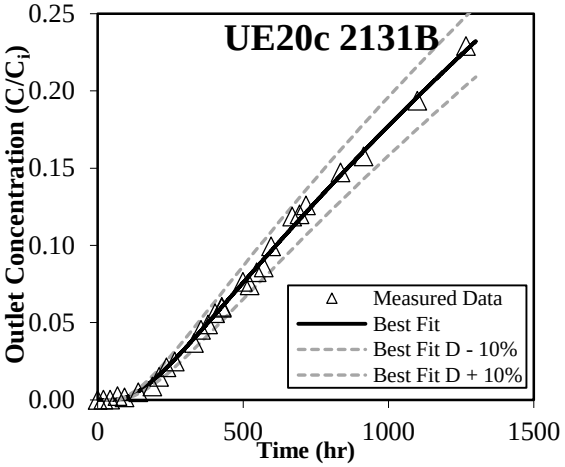
UE20c 2131B
Outlet Concentration (C/Ci)
Time (hr)
Measured Data
Best Fit
Best Fit D - 10%
Best Fit D + 10%

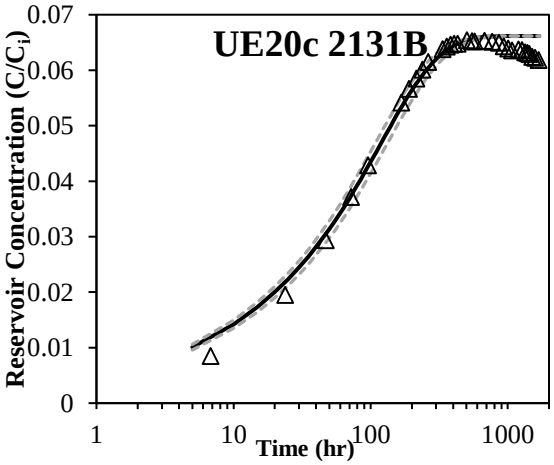
UE20c 2131B
Reservoir Concentration (C/Ci)
Time (hr)

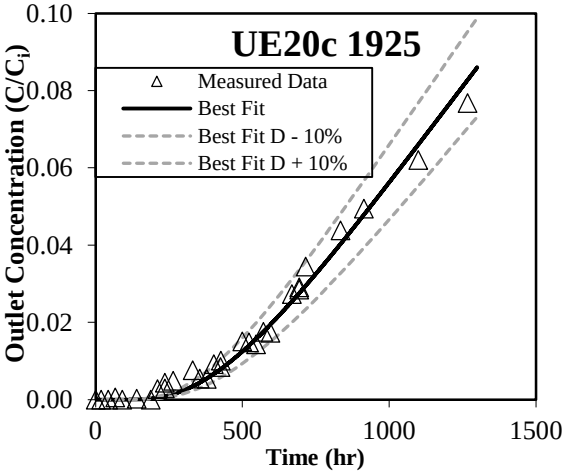
UE20c 1925
Outlet Concentration (C/Ci)
Time (hr)
Measured Data
Best Fit
Best Fit D - 10%
Best Fit D + 10%

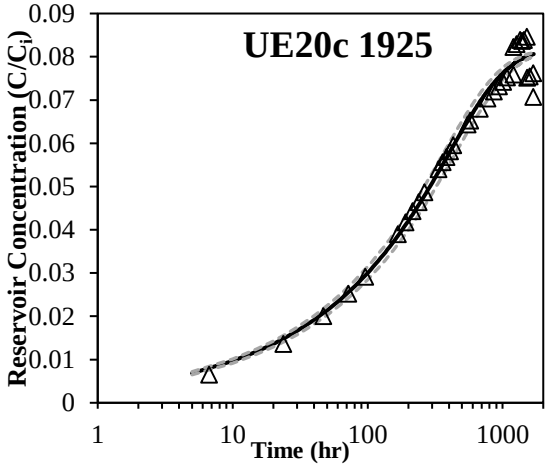
UE20c 1925
Reservoir Concentration (C/Ci)
Time (hr)

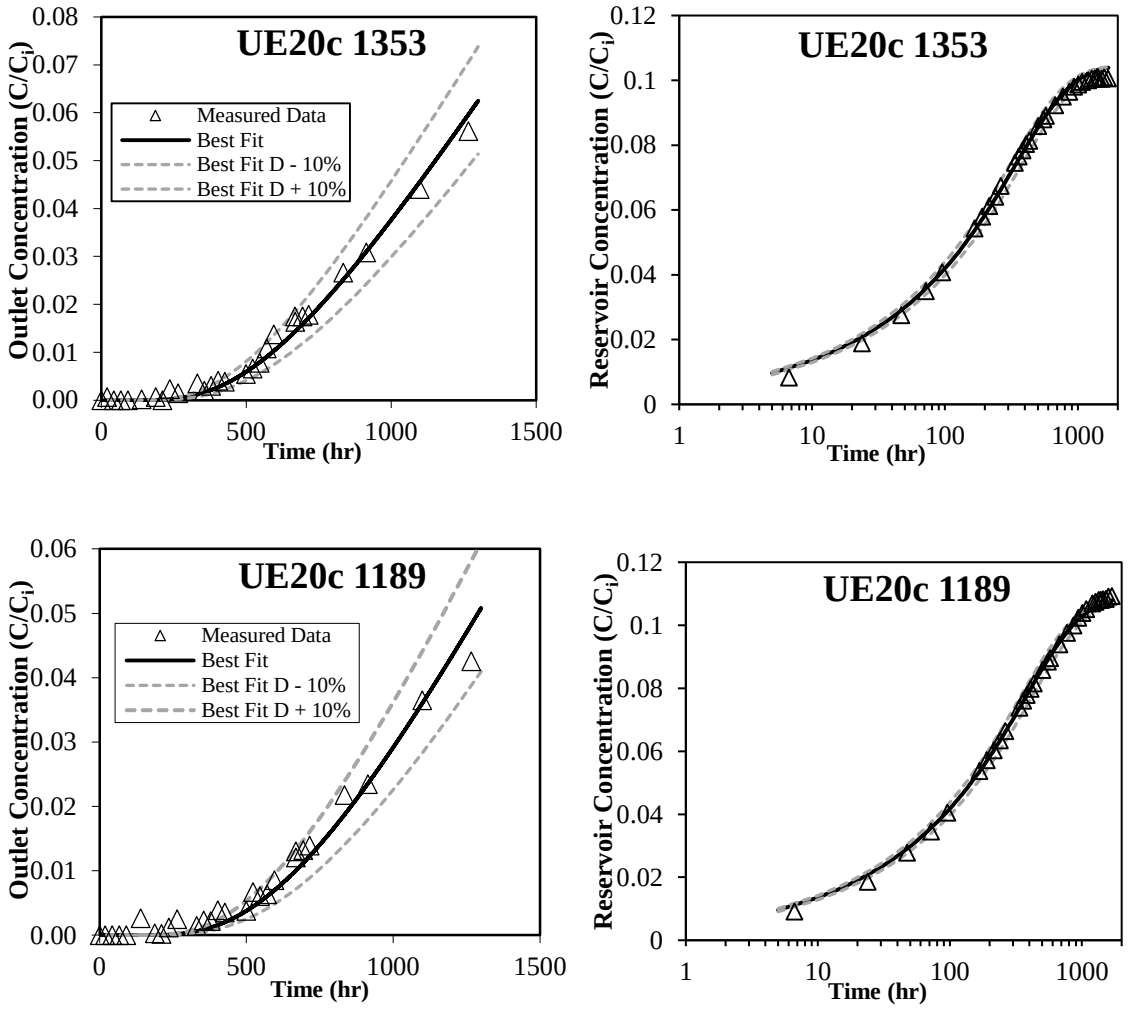

Figure 3: Diffusion Cell (Left) and Diffusion Wafer (Right) Curves showing the ratio of the tracer concentration in the measured reservoir (C) to the initial concentration (C_i) of tracer through time. The dashed lines correspond to the ±10% of the best-fitting diffusion coefficients.

To put the diffusion coefficient estimates of this study into a broader perspective, it is useful to compare them to the data set of Reimus et al. (2007), who reported diffusion coefficients measured by the diffusion cell method for 46 different rock samples from the NNSS, representing a wide range of volcanic rock lithologies, but exclude the current samples. The estimates for halides and ^{3}HHO collectively spanned nearly 2 orders of magnitude, from $0.09 \cdot 10^{-6}$ to $6.2 \cdot 10^{-6}$ cm^2/s, which is much larger than the range of values reported in this study. Figure 4 shows the values of log matrix diffusion coefficients divided by free-water diffusion coefficients (log D_m/D^*) of the 46 data points from Reimus et al. (2007) plotted against log D_m/D^* values predicted by a multiple linear regression fit to the data (Reimus et al., 2007),

$$\log {D_m}/{D^*} = 1.42 + 1.91 \cdot \varphi + 0.19 \cdot \log(k) \qquad \text{(eq 7)}$$

where φ is matrix porosity and *k* is permeability. The squared correlation coefficient for this previously established relationship is 0.542, indicating a moderate positive correlation (Reimus et al., 2007). The diffusion coefficient estimates from this study are included in Figure 4, and it is apparent that they fall within the scatter of the values predicted by eq. (7), which suggests that the new values would not have significantly altered eq. (7) if they had been considered in the multiple linear regression. However, the data from this study deviate from the positive linear trend of the previous data, and display a nearly horizontal trend. This deviation arises from the much larger range in permeability values as compared to the range in both the porosity and the diffusion coefficient for this new set of samples. The permeabilities of the samples in this study range between $3.95 \cdot 10^{-14}$ to $1.5 \cdot 10^{-17}$ m^2, whereas the computed diffusion coefficient estimates are within the same order of magnitude, and the porosities only vary between 0.13 and 0.18. Thus, the variation in the predicted diffusion coefficient value from equation 7 is predominantly dependent on permeability, which has a much greater variation than the computed diffusion coefficients (Fig. 4). Additionally, the sample with the highest permeability extends beyond the permeability range of all other samples, suggesting that the previous set of samples may not have captured all the possible ranges in permeability in NNSS rocks. This may be because the permeability of this sample was dominated by a single high-permeability channel that became apparent when the sample was saturated, whereas in the other rocks, the permeabilities appeared to be more uniformly distributed over the cross-sectional areas of the samples. It stands to reason that the diffusion behavior of a sample may not follow an established permeability trend if the permeability is dominated by a unique feature that is not representative of the bulk matrix, as appeared to be the case for the sample with the highest permeability. Thus, rocks with lithophysal cavities may not be expected to exhibit as positive of a correlation between matrix diffusion coefficients and matrix permeability as rocks with more homogeneous matrices. However, it may also be that the sample thickness in this study was too small relative to the size of the cavities to exhibit any sort of a correlation; such a relationship might emerge if all samples had thicknesses that were large relative to the largest features in the matrices. The fact that the matrix diffusion coefficients of the three lava samples were all quite similar to each other and to the tuff samples despite their large contrast in permeabilities suggests that the diffusion

coefficients may have been controlled by the properties of the lava matrix in the samples, which appeared to be quite similar in all lava samples, whereas the permeability was likely controlled by the widely varying sizes and interconnectedness of the lithophysal cavities.

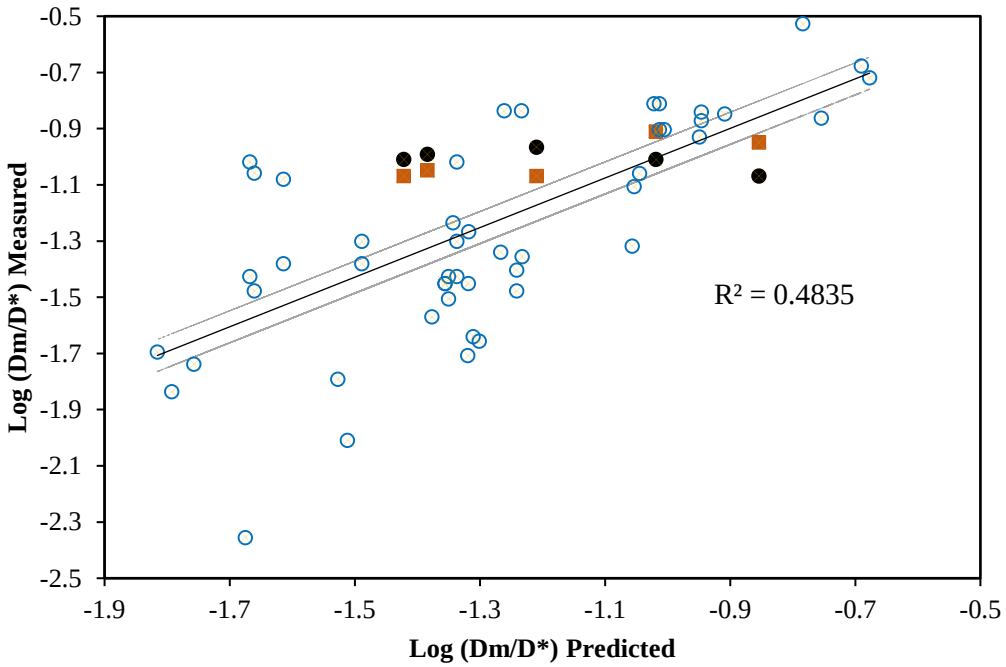

Figure 4. Log (Dm/D*) measured vs. predicted by the correlation of eq. (7). Open blue circles are the data of Reimus et al. (2007), black circles are diffusion cell estimates from this study, and brown squares are diffusion wafer estimates from this study. The black line corresponds to perfect correlation between measured and predicted values, and the grey lines correspond to the 90% confidence intervals. The R^2 value includes data from Reimus et al. (2007) and this study.

IV. Discussion

IV.A. Comparison of Method Uncertainty

Because the "true" values of the matrix diffusion coefficients of the samples are unknown, it is not possible to determine which experimental method offered the more accurate estimates of matrix diffusion coefficients. The fact that the estimates were higher for 3 of 5 samples by the diffusion cell method and higher for the other 2 samples by the diffusion wafer method indicates there is no systematic high or low bias of one method relative to the other. However, as noted previously, the data suggest that diffusion cell estimates may tend to be lower than diffusion wafer estimates when matrix permeabilities are high.

Evaluating the precision of the two methods in this study is complicated by the fact that tritiated and deuterated water were used in the two different types of respective experiments. Different analytical methods that have significantly different measurement errors were used to analyze for these isotopes. The percent standard deviation of the deuterium analysis was less than 1%, whereas the TriCarb does not report a similar quantification of error for each measurement. If sample size is a concern, however, the tritium analysis requires less sample volume than the deuterium analysis (0.5 mL vs. 2.0 mL). The use of deuterium offers clear advantages over tritium with regards to number of laboratory safety precautions required. Because of its radioactivity, the initial concentration of tritium in the diffusion cell experiments was much closer to its analytical detection limit than the initial concentration of deuterium in the wafer experiments. Consequently, there was inherently more scatter in the diffusion cell data than the diffusion wafer data. For these reasons, no attempt was made to determine and compare confidence intervals of the two sets of diffusion coefficient estimates.

Instead, the precision uncertainties associated with the two methods were qualitatively compared using a Monte Carlo-type method to simulate the data scatter that would have occurred if normally-distributed concentration measurement errors with the same relative standard deviation applied to both types of experiments. The NORMINV() function in Excel was used for the rock samples with the fastest and slowest changes in concentrations (samples UE-20c-2131.3-2131.5A (TCA) and UE-20c-1189-1189.25 (BA), respectively) to generate synthetic data sets that had the best-fitting curve as the mean and a standard deviation equal to 5% of the mean at regularly-spaced times throughout the test (Figures 5 and 6). The RAND() function, which generates uniformly-distributed random numbers between 0 and 1, served as the probability input value for the NORMINV() function to ensure that the synthetic data were normally distributed about the best-fitting curve. In Figures 5 and 6, 10 normally-distributed points are plotted at each selected sampling time along with the best-fitting curve and curves corresponding to matrix diffusion coefficients equal to ±10% of the best-fitting diffusion coefficients.

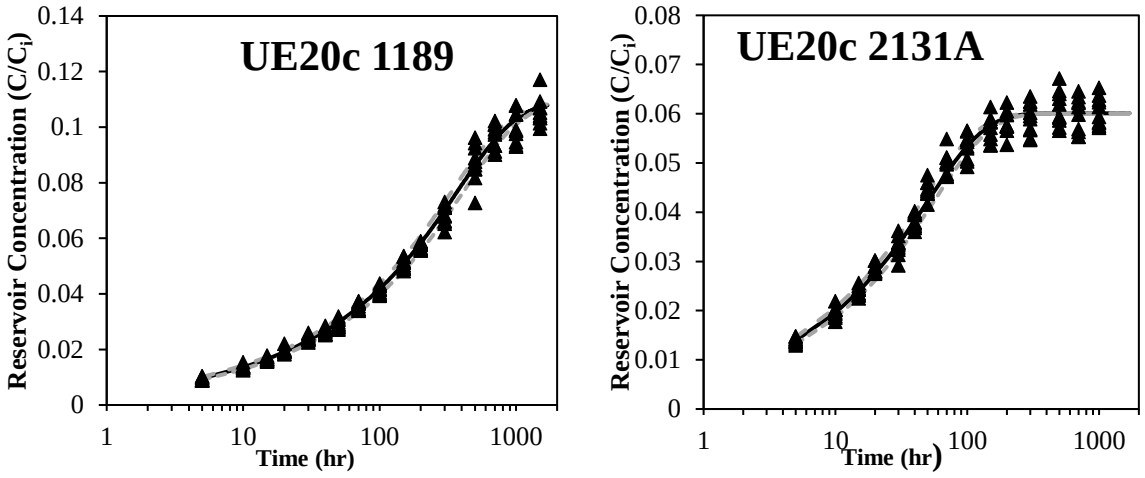

Figure 5: Normally-distributed, randomly-generated data set. Sample 1189 (left) corresponds to the diffusion wafer experiment with the slowest-changing concentrations, whereas 2131 (right) corresponds to the experiment with the fastest-changing concentrations. The mean at each time interval is equal to the value on the model curve that best fits the actual diffusion wafer data (solid line), and the standard deviation is equal to 5% of the mean. There are 10 randomly-generated data points at each time point. The dashed lines correspond to the ±10% of the best-fitting diffusion coefficients.

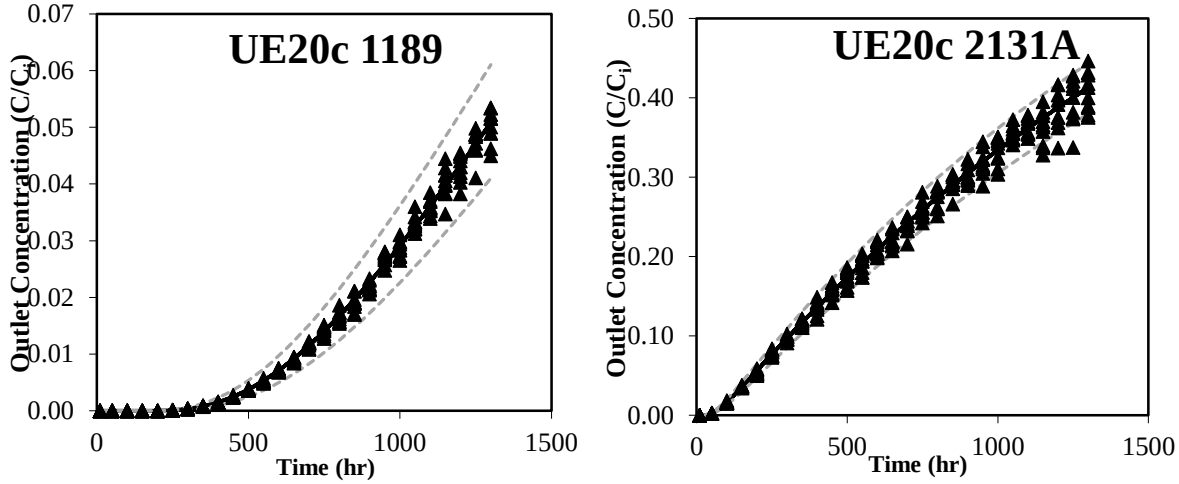

Figure 6: Normally-distributed, randomly-generated data set. Sample 1189 (left) corresponds to the diffusion cell experiment with the slowest-changing concentrations, whereas 2131 (right) corresponds to the experiment with the fastest-changing concentrations. The mean at each time interval is equal to the value on the model curve that best fits the actual diffusion cell data (solid line), and the standard deviation is equal to 5% of the mean. There are 10 randomly-generated data points at each time point. The dashed lines correspond to the ±10% of the best-fitting diffusion coefficients.

In Figures 5 and 6, it is qualitatively apparent that a 5% relative standard deviation results in more of the synthetic data points falling outside the "bands" defined by the ±10% curves in the case of the diffusion wafers than in the case of the diffusion cells. The implication is that, for the same relative random experimental errors, there will be greater uncertainty in estimating diffusion coefficients from diffusion wafer experiments than diffusion cell experiments. Thus, if the two different types of experiments were conducted in ways that result in the same relative *random* experimental errors, diffusion cell experiments can be expected to yield diffusion coefficient estimates that have less uncertainty. Greater uncertainty from the diffusion wafer method may arise from the quicker breakthrough times. The method is more sensitive to surface heterogeneities of the rock sample. Additionally, the diffusion wafer method requires occasional refilling of the reservoir, which can introduce uncertainties related to dilution corrections and volume errors. We again emphasize that no attempt was made in this study to assess and compare either the randomness or the relative magnitudes of the errors in the two different types of experiments because the different tracers and different analytical methods would have biased such a comparison.

IV.B. Comparison of Method Practicality

The diffusion wafer method appears to offer clear advantages over the diffusion cell method from the perspective of experimental apparatus simplicity. Experimental setup for the diffusion wafer method requires simply to prepare samples of constant thickness and cross-sectional area and then to seal the peripheral surface area with a silicone gel or other sealant to ensure diffusional access only to the two ends of the wafer having the same cross-sectional area. These samples are then saturated with a tracer, submersed into a stirred vessel with tracer-free water without blocking the open surfaces, and then periodically sampled. The diffusion cell method requires essentially the same rock preparation steps, plus incorporation of the sample into a barrier that will separate high- and low-concentration reservoirs, which increases the chances of compromising the sample relative to simply coating the periphery with a sealant. The diffusion cell apparatus must also be specially constructed, and its greater complexity relative to a simple beaker-type reservoir creates a greater potential for leaks. Additionally, both reservoirs of the diffusion cell must be sampled to maintain a constant head on both sides and prevent a hydraulic gradient that drives advective flow that could overwhelm diffusive flux. Kirino et al.

(2009) demonstrated a positive correlation between estimated diffusion coefficients and solution density, indicating that even with initially equal head levels, density-driven advective flow in the diffusion cell method can lead to overestimation of the diffusion coefficients and may require additional correction. It is also possible for the diffusion wafer method to be affected by advective flow if the water initially saturated into the sample is denser than the reservoir water. For both methods, the effects of advective flow will be exaggerated in more permeable rock samples.

Theoretically, the diffusion wafer experiment should produce tracer breakthrough 4 times faster than the diffusion cell method because the diffusion distance through the wafer is half that of the cell, and diffusion times scale with distance squared (eqs. 4,6). In the experiments of this study, the time needed for complete tracer breakthrough of a given sample appeared to be somewhat less than a factor of 4 between the two types of experiments. In the diffusion wafer experiments, the tracer appears almost immediately in the stirred vessel, whereas there is always a time delay in observing tracer in the low-concentration reservoir of a diffusion cell (Figure 3). It is important to note, however, that the early initial breakthrough in a diffusion wafer may only reflect the properties of the outer edges of the rock sample, and it can also be sensitive to how thoroughly the wafer surfaces are dried off before being immersed, so a full assessment of the breakthrough curve (~500-1000 hours for these samples) is necessary to calculate an accurate diffusion coefficient.

V. Conclusions

Based on the results of this study, we conclude that there is no obvious advantage in using the more widely-accepted diffusion cell method over the much simpler diffusion wafer method for estimating matrix diffusion coefficients in rock samples. The differences in the estimates provided by the two methods on the same rock samples are within about 30%, and considering that neither method produced estimates of diffusion coefficients that were either consistently higher or lower than the other, both methods should provide equally acceptable estimates for use in transport models, although a larger sample size with a greater range of permeabilities is necessary to confirm this position. This is particularly true when one considers that the internal variability of a lithologic unit's rock properties is often greater than 30%. Furthermore, when one considers that for a given time and cost, more diffusion wafer

experiments can be conducted than diffusion cell experiments, the diffusion wafer method offers the advantage that it can provide better statistical representation of a given type of rock to better address variability resulting from rock heterogeneity. It should also be noted that when accounting for the effects of matrix diffusion in fractured rocks in contaminant transport models, there is generally greater sensitivity to and greater uncertainty in average fracture apertures and distances between flowing fractures than there is to matrix diffusion coefficients (Reimus et al., 2003; Reimus et al., 2011). This has the effect of reducing any concerns about which type of experiment yields more accurate diffusion coefficient estimates, especially when they already appear to be in relatively good agreement.

Regarding implications for tritiated water transport at the NNSS, the results of this study suggest that matrix diffusion coefficients in lava flow matrices with varying sizes of lithophysal cavities are quite similar despite significant differences in the permeabilities of the samples. The implication is that the matrix in which the lithophysal cavities are embedded likely controls the diffusion coefficients. It seems logical that the differences in the measured permeabilities of the samples are probably the result of discrete flow pathways through the samples of narrow cross section relative to the sample cross section. In such cases, one would expect the bulk diffusion coefficients to be more poorly correlated with sample permeabilities than in cases where the permeability reflects that of the entire matrix.

Acknowledgements

We would like to thank George Perkins for the IRMS analysis of deuterated water. We would also like to thank Giday Woldegabriel and Nicole DeNovio for their assistance in selecting the rock samples used for this study. This work was supported by the NNSS Underground Test Area Activity, administered by the U.S. Department of Energy, Environmental Management Office. Los Alamos National Laboratory is managed and operated by Los Alamos National Security, LLC for the U.S. Department of Energy's National Nuclear Security Administration under contract DEAC52-06NA25396. UGTA TIRP Review approval: Log No. 2017-172.

References

Blankennagel, R. K., Weir, J. E., 1973. Geohydrology of the eastern part of Pahute Mesa, Nevada Test Site, Nye County, Nevada. US Government Printing Office.

Bradbury, M. H., Green, A., 1985. Measurement of important parameters determining aqueous phase diffusion rates through crystalline rock matrices. Journal of Hydrology, 82(1-2): 39-55.

Callahan, T. J., Reimus, P. W., Bowman, R. S., Haga, M .J., 2000. Using multiple experimental methods to determine fracture/matrix interactions and dispersion of nonreactive solutes in saturated volcanic tuff. Water Resources Research, 36(12): 3547-3558.

Drellack Jr, S. L., Prothro, L. B., Roberson, K. E., 1997. *Analysis of fractures in volcanic cores from Pahute Mesa, Nevada Test Site* (No. DOE/NV/11718--160). Bechtel Nevada Corp., Las Vegas, NV (United States).

Farnham, I., Rehfeldt, K., 2017. *Underground Test Area Calendar Year 2015 Annual Sampling Analysis Report Nevada National Security Site, Nevada, Revision 0.* (NO. DOE/NV-1577) Navarro, Las Vegas, NV (United States).

Finnegan, D. L., Bowen, S. M., Thompson, J. L., Miller, C. M., Baca, P. L., Olivas, L. F., Geoffrion, C. G., Smith, D. K., Goishi, W., Esser, B. K., Meadows, J. W., Namboodiri, N., Wild, J. F., 2016. *Nevada National Security Site Underground Radionuclide Inventory, 1951-1992: Accounting for Radionuclide Decay through September 30, 2012* (No. LA-UR--16-21749). Los Alamos National Laboratory, Los Alamos, NM (United States).

Freeze, R. A., Cherry, J. A., 1979. *Groundwater*, Prentice Hall, Englewood Cliffs, New Jersey, 604p.

Grisak, G. E., Pickens, J. F., 1980. Solute transport through fractured media: 1. The effect of matrix diffusion. Water Resources Research, 16(4), 719-730.

Hershey, R. L., Fereday, W., 2016. Laboratory Experiments to Evaluate Matrix Diffusion of Dissolved Organic Carbon Carbon-14 in Southern Nevada Fractured-rock Aquifers (No. 45266). Desert Research Institute, Nevada University, Reno, NV.

Kirino, Y., Yokoyama, T., Hirono, T., Nakajima, T., Nakashima, S., 2009. Effect of density-driven flow on the through-diffusion experiment. Journal of contaminant hydrology, 106(3): 166-172.

Kozaki, T., Sato, Y., Nakajima, M., Kato, H., Sato, S., Ohashi, H., 1999. Effect of particle size on the diffusion behavior or some radionuclides in compacted bentonite. Journal of Nuclear Materials, 270: 265-272.

Liu, H. H., Salve, R., Wang, J. S., Bodvarsson, G. S., Hudson, D., 2004. Field investigation into unsaturated flow and transport in a fault: model analyses. Journal of Contaminant Hydrology, 74: 39-59.

Małoszewski, P., Zuber, A., 1985. On the theory of tracer experiments in fissured rocks with a porous matrix. Journal of Hydrology, 79(3-4): 333-358.

Navarro, 2017. Written Communication. Subject: "UGTA Chemistry Database (UCDB)," UGTA Technical Data Repository Database Identification Number UGTA-4-1197. Las Vegas, NV

Neretnieks, I., 1980. Diffusion in the rock matrix: An important factor in radionuclide retardation? Journal of Geophysical Research: Solid Earth, 85(B8): 4379-4397.

Reimus, P. W., Haga, M. J., 1999. *Analysis of tracer responses in the BULLION forced-gradient experiment at Pahute Mesa, Nevada* (No. LA-13615-MS). Los Alamos National Laboratory, Los Alamos, NM (US).

Reimus, P. W., Haga, M. J., Humphrey, A. R., Counce, D. A., Callahan, T. J., Ware, S. D., 2002a. Diffusion cell and fracture transport experiments to support interpretations of the BULLION forced-gradient experiment. LA-UR-02-6884. Los Alamos National Laboratory, Los Alamos, NM.

Reimus, P. W., Ware, S. D., Benedict, F. C., Warren, R. G., Humphrey, A. J., Adams, A. I., Wilson, B., Gonzales, D., 2002b. Diffusive and advective transport of 3H, 14C, and 99Tc in saturated, fractured volcanic rocks from Pahute Mesa, Nevada. LA-13891-MS. Los Alamos National Laboratory, Los Alamos, NM.

Reimus, P., Pohll, G., Milheve, T., Chapman, J., Haga, M., Lyles, B., Kosinski, S., Niswonger, R., Sanders, P., 2003. Testing and parameterizing a conceptual model for solute transport in a fractured granite using multiple tracers in a forced-gradient test. Water Resources Research, 39(12): 1356.

Reimus, P. W., Hershey, R. L., Decker, D. L., Ware, S. D., Papelis, C., Earman, S., Abdel-Fattah, A., Haga, M., Counce, D., Chipera, S., Sedlacek, C., 2006. Tracer transport properties in the lower carbonate aquifer of Yucca Flat. Los Alamos National Laboratory LA-UR-06-0486, Los Alamos, NM.

Reimus, P. W., Callahan, T. J., Ware, S. D., Haga, M. J., Counce, D. A., 2007. Matrix diffusion coefficients in volcanic rocks at the Nevada test site: Influence of matrix porosity, matrix permeability, and fracture coating minerals. Journal of contaminant hydrology, 93(1): 85-95.

Reimus, P. W., Duke, C. L., Roback, R. C., 2011. Translation of field tracer-test results into bounding predictions of matric diffusion in the shallow subsurface at Idaho National Laboratory, USA. Hydrogeology Journal, 19: 1021-1037.

Robinson, B. A., Houseworth, J. E., Chu, S., 2012. Radionuclide transport in the unsaturated zone at Yucca Mountain, Nevada. Vadose Zone Journal, 11(4).

Skagius, K., Neretnieks, I., 1986. Porosities and diffusivities of some nonsorbing species in crystalline rocks. Water Resources Research, 22(3): 389-398.

Tang, D. H., Frind, E. O., Sudicky, E. A., 1981. Contaminant transport in fractured porous media: Analytical solution for a single fracture. Water Resources Research, 17(3): 555-564.

Thomson, J., 2001. Use and preparation of quench curves in liquid scintillation counting. Packard BioScience Company, Meriden, Connecticut.

Appendix: Selection and photos of rock wafers

The core selection process for this diffusion study was intended to focus on hydrogeologic units (HGUs) believed to host important flow pathways at Pahute Mesa that also lacked or were under-represented in matrix diffusion coefficient data. Matrix diffusion data are considered important for Pahute Mesa (PM) contaminant boundary calculations because tritium is the radionuclide with the greatest potential for defining the contaminant boundary from Pahute Mesa sources, and the only credible mechanism for retardation of tritium along flow pathways is matrix diffusion. Prior to undertaking the study, the Tiva Canyon tuff (TCA), Benham Aquifer lava flows (BA), and the Belted Range Aquifer (BRA) were identified as potentially hosting important PM flow pathways and lacking matrix diffusion coefficient data. During preliminary discussions, it also became apparent that there was considerable uncertainty in predicting or accounting for the influence of lithophysal cavities on matrix diffusion coefficients. No previous diffusion studies used for the Underground Test Area (UGTA) Activity had focused on these features, which are prevalent in lava flow units and also occur in some tuffs. Thus, particular attention was given to looking for samples that contained lithophysal cavities, with emphasis on the BA lava flows.

The first step in the sample selection process was to obtain maps and listings of cored intervals and associated lithologic descriptions from various coreholes from PM. After intervals of interest were identified, an attempt was made to obtain archived photos of core boxes containing the intervals from the USGS Mercury Core Library and Data Center website. When available, the photos proved extremely useful in the selection process because they allowed a quick determination of whether the core of interest was suitable for matrix diffusion experiments (i.e., intact blocks of sufficient size). An example of one of the core box photos, containing one of the intervals ultimately selected for testing, is shown in Fig. A-1. When photos were not available, the intervals of interest were directly examined at the USGS core library in Mercury, NV. Samples selected to be shipped to LANL for further consideration included Tiva Canyon tuff samples from coreholes UE-20c and UE-20f, Scrugham Peak lava samples from UE-20d, lava samples from Calico Hills borehole ER-20-6#1, and Benham Aquifer rhyolitic lava samples from UE-20c. No BRA material was selected because no suitable core for this unit was identified, and also because it was decided that the other units had greater importance for flow and transport models.

Once the selected core arrived at LANL, it was down-selected for the diffusion experiments. Ultimately, four BA rhyolitic lava flow samples and one moderately-welded TCA tuff core sample were selected for the experiments, all from corehole UE-20c. Diffusion cell experiments had already been conducted on lava samples from the Calico Hills (Reimus et al., 2002a), and samples from the Scrugham Peak lava were considered confining units and thus of less interest for the diffusion experiments. Of the TCA tuff samples, the samples from borehole UE-20f were considered to be more densely welded and of less interest than the TCA tuff samples from UE-20c.

The down-selected core was processed in the manner described in the body of the report, with the TCA core being processed into two adjacent samples from the same original block of

core to allow testing of a "duplicate." Figure A-2 shows the down-selected samples as they arrived at LANL, and Figures A-3 to A-7 show each of the samples after processing for diffusion experiments. Processing of one of the four BA rhyolitic lava flow samples was abandoned because it contained lithophysal cavities that were so big it was impossible to obtain a sample that was not completely transected by a cavity, which was considered non-representative for matrix diffusion measurements.

LANL then conducted the proof-of-concept experiments described in the body of the report to compare diffusion coefficients measured on each sample using two different methods, a conventional diffusion cell approach and a diffusion wafer approach. In addition to filling data gaps for PM HGUs that lack diffusion coefficient data, these experiments had the goal of determining whether the less-costly and faster diffusion wafer approach could be applied to NNSS samples so that additional data needs, including assessments of statistical variability in diffusion coefficients, could be more efficiently addressed in the future.

Figure A-1. Photo of core from UE-20c 2125-2133 ft below surface (Tiva Canyon tuff):

Figure A-2. Five samples obtained from UE-20c. The first four are rhyolitic lavas from the Benham Aquifer. The third sample was excluded because of its large void space. The fifth sample is a Tiva Canyon tuff.

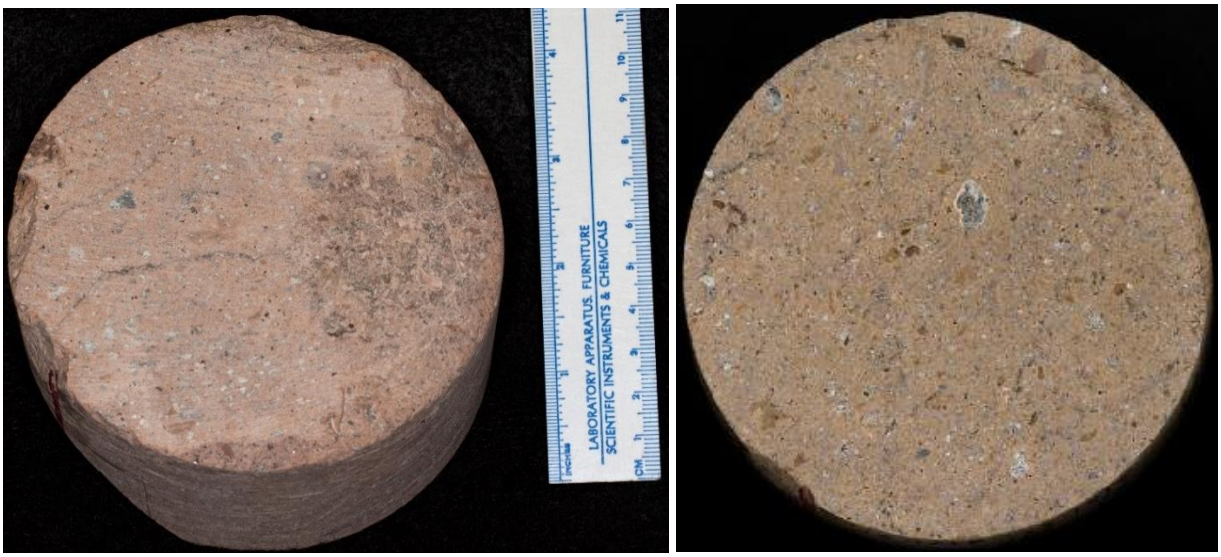

Figure A-3. Unprocessed (left) and cut/processed (right) sample from UE-20c-2131.3-2131.5 ft below surface (Tiva Canyon Tuff). Sample on right designated UE-20c-2131.3-2131.5A.

Figure A-4. Second cut/processed sample from UE-20c-2131.3-2131.5 ft below surface (Sample UE-20c- 2131.3-2131.5B). Sample before processing is shown in Figure A-3, left.

Figure A-5. Unprocessed (left) and cut/processed (right) sample from UE-20c-1925.1-1925.3 ft below surface (Benham Aquifer lava).

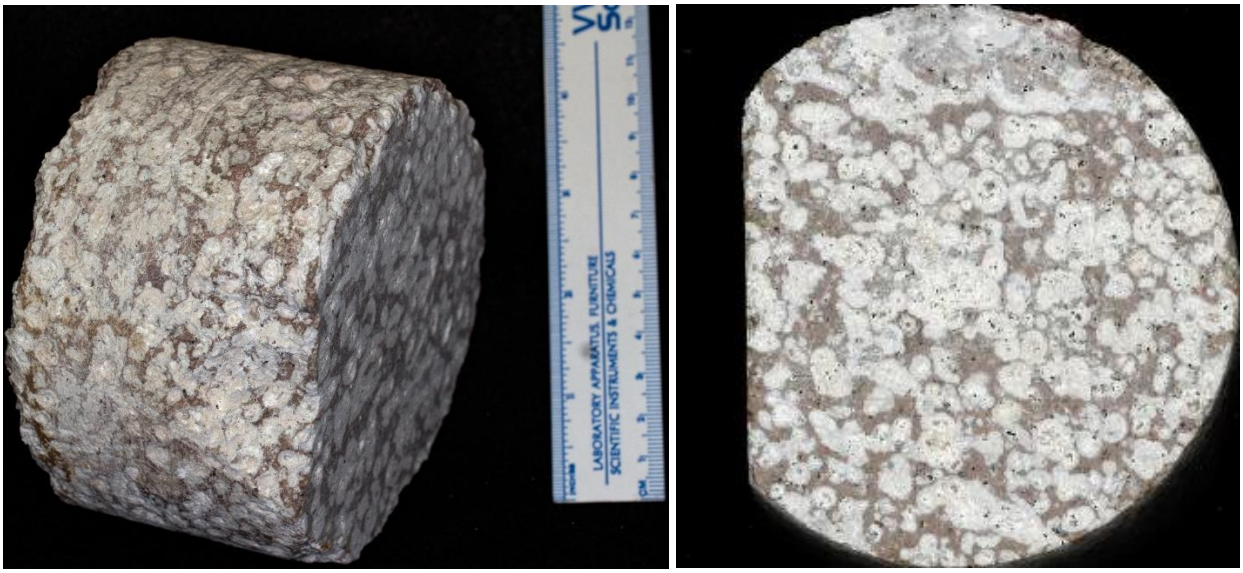

Figure A-6. Unprocessed (left) and cut/processed (right) sample from UE-20c-1353-1353.28 ft below surface (Benham Aquifer lava).

Figure A-7. Unprocessed (left) and cut/processed (right) sample from UE-20c-1189-1189.25 ft below surface (Benham Aquifer lava).